Center for Turbulence Research
Proceedings of the Summer Program 2006

Green's function discretization of Pridmore-Brown wave operator

By D. Casalino† AND D. Bodony

A numerical method is presented for sound transmission through non-uniform flows with no restrictions on the ratio between the flow variation scale and the acoustic wavelength. Because it is based on the solution of a third-order convective linear wave equation for the pressure perturbation in the frequency domain, the method described on the following pages can be applied in the vortex sheet limit without any treatment of the wake shed by a trailing edge under sound excitation. This is an idealized representation of an aero-engine exhaust where noise generated by the fan system is transmitted through the annular bypass duct, diffracted by the duct lip, refracted by the external bypass stream, and radiated to the far field. The wave equation is obtained by linearization of the acoustic analogy equation put forth by Lilley (1974) around a time-independent base flow. The main interest of this formulation is not in the proper separation between sound propagation and generation, which is indeed unambiguous only for a unidirectional transversely sheared base flow, but in the wave operator itself, originally derived by Pridmore-Brown (1958). The numerical scheme is based on the Green's function discretization technique previously developed for a second-order equation for the acoustic potential, and herein extended to Pridmore-Brown wave operator in order to avoid any explicit treatment of the potential discontinuity across the vortex sheet in turbofan bypass noise predictions.

1. Introduction

In modern high bypass ratio turbofan engines at high power operating conditions, the aft radiated fan noise is an important noise source, in some cases overwhelming the jet mixing noise. Due to the presence of a shear layer between the bypass and the external stream, the numerical simulation of aft fan noise is a challenging task. In fact, while satisfactory for noise radiation from the intake, methods based on the solution of second-order wave equations for the acoustic potential in the frequency domain are inadequate for the prediction of noise radiation from the exhaust, as pointed out by Druon *et al.* (2004). Two convected wave equations are commonly used for nacelle noise predictions. The first one, derived by Pierce (1990), is valid for background rotational flows, but only for those that vary slowly over the length and time scale of the sound waves (high-frequency approximation). The second equation is obtained by linearization of the compressible full potential equation, as shown by Di Francescantonio & Casalino (1999), among others, and is therefore only valid for irrotational base flows. Extensions to vortical base flows, as proposed by Bergliaffa *et al.* (2004), may have a practical relevance in the future. In this scenario, the solution of the linearized Euler equations in the time domain seems to be the only viable solution to the problem. However, due to the computational cost and to the occurrence of instability waves of hydrodynamic nature in the shear layer that contaminate the acoustic solution, the industrial relevance of this numerical approach is still questionable.

† CIRA, Italian Aerospace Research Center, Capua 81043, Italy

The theoretical and numerical modeling of jet mixing noise has previously required the formulation of acoustic analogies that, with the intention of separating propagation and generation effects, incorporate the unequal convection velocities on the two sides of the mixing layer and other mean flow refraction effects in the wave operator. The equation derived by Lilley (1974) for the logarithm of the pressure, after linearization about a time-independent unidirectional transversely sheared base flow, as illustrated by Colonius *et al.* (1997), provides the proper theoretical separation between noise propagation and generation. Even in this case, however, an unambiguous separation requires further assumptions. Since any acoustic analogy formulation is an exact rearrangement of the flow equations into a wave equation with discarded terms gathered at the right-hand side and interpreted as source terms, the separation between propagation and generation is not strictly required when the acoustic analogy is used in connection with a numerical simulation of the source terms. However, as recently demonstrated by Freund *et al.* (2004), the proper inclusion of the mean flow refraction effects in the wave operator at the left-hand side is crucial for the robustness of the formulation, that is, its sensitivity to modeling errors in the source terms. The present work is based on this statement, together with the intention of assessing the practical relevance of Lilley's wave operator for a generic sheared base flow, even in the vortex sheet limit (low frequency limit) as an alternative to the solution of linearized Euler equations.

The objective of this paper is to develop a numerical approach based on the Green's function discretization (GFD) method applied to a third-order wave operator acting on the pressure perturbation about a generic three-dimensional background flow, as described in § 2. The GFD method, previously developed for the solution of a second-order convected wave equation for the acoustic potential (Di Francescantonio & Casalino (1999), Casalino *et al.* (2004), Casalino *et al.* (2006)), can be classified as a wave-based unstructured finite difference method. As illustrated in § 3, the method is based on a local interpolation formula obtained as a combination of local approximate elementary solutions. After collocation on the stencil nodes and inversion, a discretization formula for the spatial derivatives of the unknown variable can be obtained. Only a preliminary verification of the numerical approach is presented in § 4 by comparing present results with other results available in the literature. Further analysis is necessary in order to demonstrate the practical relevance of the method for the simulation of noise radiation from turbofan exhaust configurations at realistic operating conditions.

2. Governing equation and boundary conditions

By combining the mass and linear momentum conservation equations in a compressible fluid and neglecting viscous effects, Lilley (1974) obtained a third-order wave equation:

$$\frac{\mathrm{D}}{\mathrm{D}t}\left[\frac{\mathrm{D}^2\Pi}{\mathrm{D}t^2}-\frac{\partial}{\partial x_j}\left(c^2\frac{\partial\Pi}{\partial x_j}\right)\right]+2\frac{\partial u_k}{\partial x_j}\frac{\partial}{\partial x_k}\left(c^2\frac{\partial\Pi}{\partial x_j}\right)=-2\frac{\partial u_j}{\partial x_k}\frac{\partial u_i}{\partial x_j}\frac{\partial u_k}{\partial x_i} \tag{2.1}$$

where $\Pi=(1/\gamma)\ln p$. In Eq. (2.1) and throughout this paper p, ρ, T, c and u_i denote the flow pressure, density, temperature, sound speed and Cartesian velocity components, respectively. The fluid is assumed to be an ideal gas so that $c^2=\gamma p/\rho=\gamma RT$, where γ and R are the ratio of specific heats and the gas constant, respectively.

Since Lilley's equation is nonlinear, a common practise is to linearize it around a time-independent base flow, subtracting the base flow balance and adding all terms removed from the linearized left-hand side to the source terms at the right-hand side. The resulting linear equation is thus still exact, all the nonlinear terms being interpreted as source terms. In the framework of jet mixing noise simulation, a significant interest is devoted

to the analysis and numerical modeling of the source terms arising in Lilley's acoustic analogy equation (Colonius *et al.* (1997)). In the present work, however, the noise excitation is only prescribed via boundary conditions or elementary model sources. The only interest is therefore in the wave operator and not in the aeroacoustic source terms. The following homogeneous linear wave equation is thus considered:

$$\frac{\mathrm{D}_0}{\mathrm{D}t}\left[\frac{\mathrm{D}_0^2\Pi'}{\mathrm{D}t^2}-\frac{\partial}{\partial x_j}\left(c_0^2\frac{\partial\Pi'}{\partial x_j}\right)\right]+2\frac{\partial U_k}{\partial x_j}\frac{\partial}{\partial x_k}\left(c_0^2\frac{\partial\Pi'}{\partial x_j}\right)=0 \tag{2.2}$$

where $\mathrm{D}_0/\mathrm{D}t$ is the mean-velocity Lagrangian derivative, $\Pi'=(1/\gamma)\,p'/p_0$, p' is the pressure perturbation, and p_0, T_0, c_0 and U_i denote base flow quantities. Then, assuming harmonic perturbations of radian frequency ω and using the Lagrangian derivative $\mathrm{D}_0/\mathrm{D}t=-\mathrm{i}\,\omega+U_i\,\partial/\partial x_i$, Eq. (2.2) takes the following final form:

$$\begin{aligned}
&\mathrm{i}\,k^3\Pi'-3\,k^2\tilde{U}_i\frac{\partial\Pi'}{\partial x_i}-3\,\mathrm{i}\,k\,\tilde{U}_i\tilde{U}_j\frac{\partial^2\Pi'}{\partial x_i\partial x_j}-3\,\mathrm{i}\,k\left(\tilde{U}_j\frac{\partial\tilde{U}_i}{\partial x_j}\right)\frac{\partial\Pi'}{\partial x_i}\\
&+\tilde{U}_k\frac{\partial}{\partial x_k}\left(\tilde{U}_i\tilde{U}_j\frac{\partial^2\Pi'}{\partial x_i\partial x_j}\right)+\tilde{U}_k\frac{\partial}{\partial x_k}\left[\left(\tilde{U}_j\frac{\partial\tilde{U}_i}{\partial x_j}\right)\frac{\partial\Pi'}{\partial x_i}\right]+\mathrm{i}\,k\frac{\partial\tilde{T}}{\partial x_j}\frac{\partial\Pi'}{\partial x_j}\\
&+\mathrm{i}\,k\,\tilde{T}\frac{\partial^2\Pi'}{\partial x_j^2}-\tilde{U}_k\frac{\partial}{\partial x_k}\left(\frac{\partial\tilde{T}}{\partial x_j}\frac{\partial\Pi'}{\partial x_j}+\tilde{T}\frac{\partial^2\Pi'}{\partial x_j^2}\right)+2\frac{\partial\tilde{U}_k}{\partial x_j}\left[\frac{\partial\tilde{T}}{\partial x_k}\frac{\partial\Pi'}{\partial x_j}+\tilde{T}\frac{\partial^2\Pi'}{\partial x_k\partial x_j}\right]=0
\end{aligned} \tag{2.3}$$

where $k=\omega/c_\infty$ is the acoustic wavenumber, and $\tilde{U}_i=U_i/c_\infty$ and $\tilde{T}=T_0/T_\infty$ are base flow quantities made dimensionless by free stream reference conditions. In the present work, a generic three-dimensional base flow is considered, thus the spatial derivatives in Eq. (2.3) are further distributed on all the Cartesian velocity components.

The system of governing equations is completed by a zero normal derivative condition on rigid walls, and by a Sommerfeld radiation condition on far field boundaries. The radiation condition is used in connection with a perfect matched layer (PML) technique in order to attenuate the outgoing acoustic waves and minimize inward spurious reflections. The Sommerfeld radiation condition is a Robin-type condition in which the Dirichlet-to-Neumann (DtN) factor is obtained for a plane wave propagating in a uniform flow, and by approximating the radiation vector with the normal vector $\mathbf{n}$ to the boundary. Hence the radiation condition reads:

$$\partial\Pi'/\partial n-\mathcal{M}\,\Pi'=\partial\Pi'_{\mathrm{inc}}/\partial n-\mathcal{M}\,\Pi'_{\mathrm{inc}} \tag{2.4}$$

where $\mathcal{M}=\mathrm{i}\,k\sqrt{T_\infty/T}\left(-M_n+\sqrt{M_n^2+\beta^2}\right)/\beta^2$ is the DtN factor, $M_n=\mathbf{U}\cdot\hat{\mathbf{n}}/c$ is the mean flow Mach number projected on the outward normal direction, β is the Prandtl-Glauert factor and Π'_{inc} is a prescribed acoustic incident field.

The PML technique, proposed by Berenger (1994) for computational electro-magnetic, has been recently applied to the convective Helmholtz equation by Hu (2004) and Bécache *et al.* (2004), among others. It is based on the idea that the wave equation in a layer close to the radiation boundary can be modified by introducing a dissipation term, whose effect is to transform an outgoing propagating wave into an outgoing evanescent wave, without spurious backward reflections. Consider, as a matter of convenience, a uniform flow of Mach number M parallel to the x-axis. The propagation of harmonic acoustic perturbations is governed by the convected wave equation $\beta^2\,p'_{xx}+p'_{yy}+p'_{zz}+\mathrm{i}\,2\,k\,M\,p'_x+k^2\,p'=0$. This can be converted into a Helmholtz equation $\nabla^2_\star p'_\star+k^2p'_\star=0$ by using a Prandtl-Glauert transformation of the form: $p'(\mathbf{x})=p'_\star(\mathbf{x})\,\exp\!\left(-\mathrm{i}\,kMx/\beta^2\right)$, $x^\star=\beta^2x$, $y^\star=$

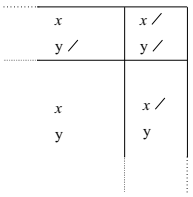

FIGURE 1. Illustration of a computational domain with PML buffer layers.

βy, $z^\star = \beta z$. A PML layer for a wave propagating in the x-direction can be now obtained by introducing the so-called PML complex change of variable $\partial/\partial x^\star \rightarrow \alpha(x^\star)\,\partial/\partial x^\star$, with $\alpha(x^\star) = 1/\left[1 + \mathrm{i}\,\sigma_x/\left(k\,c_\infty\right)\right]$. Finally, returning to original variables, and considering a generic uniform flow and a rectangular domain as sketched in Fig. 1, the full set of PML transformations reads $\partial/\partial x_i \rightarrow \alpha_i(x_i)\,\partial/\partial x_i + \mathrm{i}\,\lambda_i$ with $\lambda_i = -k\,M_i/\beta^2$. In order to ensure a smoother transition from the physical domain to the i-th PML buffer, the damping factors are increased from zero to a maximum value at the external boundary with law $\sigma_i/\left(kc_\infty\right) = \tilde{\sigma}_i^{\max}\, x_i^{\star\, n}$, where $x_i^\star$ is a normalized coordinate varying from 0 to 1 in the i-th buffer away from the computational domain. The modified wave equation and the modified radiation condition are then obtained from Eqs. (2.3) and (2.4) by substitution of the following transformed derivatives:

$$\partial_i p' \rightarrow \alpha_i\,\partial_i p' + \mathrm{i}\;\lambda_i\,p' \tag{2.5}$$

$$\partial^2_{ij} p' \rightarrow \alpha_i\alpha_j\,\partial^2_{ij} p' + \mathrm{i}\;\lambda_j\,\alpha_i\,\partial_i p' + \mathrm{i}\;\lambda_i\,\alpha_j\,\partial_j p' - \lambda_i\,\lambda_j\,p' \tag{2.6}$$

$$\begin{aligned}\partial^3_{ijk} \rightarrow\ & \alpha_i\alpha_j\alpha_k\,\partial^3_{ijk} + \mathrm{i}\;\lambda_i\,\alpha_j\,\alpha_k\,\partial^2_{jk} p' + \mathrm{i}\;\lambda_j\,\alpha_k\,\alpha_i\,\partial^2_{ki} p' + \mathrm{i}\;\lambda_k\,\alpha_i\,\alpha_j\,\partial^2_{ij} p' \\ & - \lambda_i\,\lambda_j\,\alpha_k\,\partial_k p' - \lambda_j\,\lambda_k\,\alpha_i\,\partial_i p' - \lambda_k\,\lambda_i\,\alpha_j\,\partial_j p' - \mathrm{i}\,\lambda_i\,\lambda_j\,\lambda_k\,p'\end{aligned} \tag{2.7}$$

When an incident external field is considered, the PML treatment is applied to the reflected waves by solving in the PML buffer a non-homogeneous wave equation of the form $\mathcal{L}(\Pi') = \mathcal{L}(\Pi'_{\mathrm{inc}})$, where $\mathcal{L}$ is the transformed linear wave operator.

When the free stream is not uniform, instabilities may arise in the PML buffer due to the fact that, as pointed out by Hu (2005), the above expression of λ factor does not ensure a consistency in the phase and group velocities of the linear waves. In this case, instead of finding a proper space-time transformation that ensures stability, it is more convenient to set λ to zero. A marginal stability is thus ensured by the use, instead of a crude $\Pi' = 0$ condition, of the modified radiation condition that requires smaller values of the damping factor σ.

3. Numerical scheme

The GFD scheme is based on the interpolation formula for the Helmholtz equation proposed by Caruthers *et al.* (1995). This is first adapted to a convected wave propagation, and then is used to obtain a discretization scheme for a second-order non-uniform convected wave equation under the local uniformity assumption. The same technique can be extended, without any substantial modification, to discretize the third-order wave Eq. (2.3).

Consider a generic volume $\mathcal{V}_m$ in which the acoustic pressure p' satisfies the convected Helmholtz equation (Eq. (2.3) for a uniform base flow), and suppose that the values $p'_m = p'(\mathbf{x}_m)$ are prescribed at a certain number M of points $\mathbf{x}_m$ in $\mathcal{V}_m$. We are interested in modeling the acoustic field $p'(\mathbf{x})$ in $\mathcal{V}_m$ by using these M prescribed values. Following the work of Caruthers *et al.* (1995), the pressure field is supposed to be generated by an

arbitrary distribution of N elementary sources, each with magnitude γ_n and location $\mathbf{x}_n$, i.e.,

$$p'(\mathbf{x}) = \sum_{n=1}^{N} \gamma_n \, G(\mathbf{x}, \mathbf{x}_n; \mathbf{M}) \tag{3.1}$$

where $G(\mathbf{x}, \mathbf{x}_n; \mathbf{M})$ is the Green's function of the convected Helmholtz equation. Setting $r = |\mathbf{x} - \mathbf{x}_n|$, $M_r = \mathbf{M} \cdot (\mathbf{x} - \mathbf{x}_n)/r$ and $\beta = \sqrt{1 - M^2}$, it reads:

$$G(\mathbf{x}, \mathbf{x}_n; \mathbf{M}) = \exp\left[\mathrm{i}\, kr \left(-M_r + \sqrt{M_r^2 + \beta^2}/\beta^2\right)\right] / \left(r\sqrt{M_r^2 + \beta^2}\right), \tag{3.2}$$

the constant having been absorbed in γ_n. Requiring the satisfaction of Eq. (3.1) at each point $\mathbf{x}_m$ yields a set of M compatibility conditions $p'_m = \sum_{n=1}^{N} \gamma_n \, G_{mn}$, where $G_{mn} = G(\mathbf{x}_m, \mathbf{x}_n; \mathbf{M})$. Hence, prescribing the source locations $\mathbf{x}_n$, for instance, on the surface of a sphere centered in $\mathbf{x}$, leads to a linear system that relates the N unknowns γ_n to the M values p'_m. Although a unique solution can exist only if $N = M$, Caruthers *et al.* (1995) suggested using $N > M$ in order to improve the quality of the field reconstruction in $\mathcal{V}_m$. Indeed, among the infinite solutions γ_n we can choose that one ensuring the field reconstruction with a minimum phase cancelation. This amplitude distribution is reasonably expected to satisfy a condition of minimum variation in the norm L^2 (minimum $\sum_n \gamma_n^2$), a condition that can be implicitly imposed by computing the pseudoinverse matrix G^I_{nm} of G_{mn}. The source magnitudes are thus given by $\gamma_n = \sum_{m=1}^{M} G^I_{nm} \, p'_m$ and substituting into Eq. (3.1) yields:

$$p'(\mathbf{x}) = \sum_{m=1}^{M} F_m(\mathbf{x}) \; p'_m \tag{3.3}$$

where the functions $F_m(\mathbf{x}) = \sum_{n=1}^{N} G^I_{nm} \, G(\mathbf{x}, \mathbf{x}_n)$ play the role of shape functions tailored to the local acoustic problem. Equation (3.3) is the interpolation formula proposed by Caruthers *et al.* (1995), with a minor modification to account for the convective effects.

Consider a discretized domain and let $\mathbf{x}^i_m$ denote one of the M^i stencil nodes about the node $\mathbf{x}^i$. The interpolation formula in Eq. (3.3) can be regarded as a compatibility condition between the pressure perturbation at the M^i nodes. Since the satisfaction of the convected Helmholtz equation is ensured by the fact that the shape functions $F_m(\mathbf{x})$ are combinations of elementary solutions of the same governing equation, a solution can be obtained by only requiring the verification of some boundary conditions. This is the approach used by Caruthers *et al.* (1995) that leads to the discretization scheme:

$$\sum_{m=1}^{M^i} a^i_m \, p^i_m = 0, \quad \text{with} \quad a^i_m = \begin{cases} 1 & \text{if } \mathbf{x}^i_m \equiv \mathbf{x}^i \\ -F^i_m & \text{otherwise} \end{cases} \tag{3.4}$$

where the influence coefficients of $F^i_m = F_m\big(\mathbf{x}^i\big)$ must be computed by excluding the node i from its stencil node list. Numerical results show that this GFD scheme is able to reconstruct an acoustic field with only 2 to 3 points per wave. However, it can be applied only when the Green's function of the governing equation is known, or when it can be computed in approximate forms (Caruthers *et al.* (1995)).

A more general approach consists in effectively discretizing Eq. (2.3) and the boundary conditions by means of shape functions for the derivatives of $p'(\mathbf{x})$, obtained by differentiating the shape functions $F_m(\mathbf{x})$. For example, the first order x derivative reads $p'_x(\mathbf{x}) = \sum_{m=1}^{M} F_{mX}(\mathbf{x}) \; p'_m$, with $F_{mX}(\mathbf{x}) = \sum_{n=1}^{N} G^I_{nm} \, G_x(\mathbf{x}, \mathbf{x}_n; \mathbf{M})$. Therefore, using a

collocation technique to discretize Eq. (2.3) yields a linear system $\sum_{m=1}^{M^i} a_m^i \, p'^i{}_m = 0$. A greater accuracy is ensured by considering the node i among the M^i nodes of its stencil. In this case the influence coefficients F_m^i are Kronecher delta.

Obviously, when the flow is uniform, the wave operator discretization coefficients a_m^i are identically null, since are obtained by differentiating elementary solutions of the same governing equation. Some corrective action is therefore necessary for the method to make sense. The strategy commonly adopted is to distribute the fictitious sources upon two spheres, the first having a smaller radius and supporting a larger number of sources, the second with a greater radius and only few sources. This second sphere is indeed a four-dimensional hypersphere, and a four-dimensional norm is used to evaluate the term $r = |\mathbf{x}_n - \mathbf{x}|$ in the Green's function. This prevents the shape functions from being exact solutions of the governing equation, without corrupting their suitability to model the local sound field. When applied to two-dimensional wave propagation problems, the two-dimensional Green's function is used to build the shape functions, with fictitious sources distributed upon a circle and upon a three-dimensional sphere. In the present paper 33 sources on a hypersphere of radius $10^3\lambda$, with λ denoting the acoustic wavelength, and 134 sources on a sphere of radius $10^2\lambda$ are used for three-dimensional computations, whereas 11 sources on a sphere of radius $10^3\lambda$ and 100 sources on a circle of radius $10^2\lambda$ are used for two-dimensional computations.

An interesting aspect of the GFD method is that, for each computational stencil, both the number of nodes and their location with respect to the collocation node i are arbitrary. Therefore, the method is well suited for multi-element unstructured grids. Another interesting aspect of the method is that, since the shape functions are tailored to the local acoustic problem, two computational stencils that are geometrically identical may have different discretization coefficients, depending on the wavenumber and the local base flow. In other words, the GFD shape functions can describe only a specific set of functions that locally satisfy the wave equation for a given wavenumber. Therefore, even if the mesh were greatly refined, it would be impossible to reconstruct a generic field (e.g., a constant one), which is not a solution of the wave equation for a non-zero wavenumber. A corollary is that the sum of the discretization coefficients of a generic derivative is not identically zero. This fundamental property that allows the reconstruction of a constant function is violated by the GFD scheme since a constant field is not a solution of a wave equation.

4. Verification of the numerical method

4.1. *Sound transmission through a constant area duct*

The purpose of this verification test is to check the consistency of the discretization scheme in the simple case of a uniform stream, when Eq. (2.3) reduces to a third-order convected Helmholtz equation. Comparing the numerical error with respect to the analytical solution to the same error obtained by solving the second-order convected Helmholtz equation, highlights the effect of the discretization error due to the higher order derivative. A spinning mode of azimuthal and radial mode orders $(5, 2)$ is transmitted through a rigid annular duct of inner/outer radius ratio $r_i/r_o = 0.5$, axial length $L_z = 1.13\, r_0$, crossed by a constant flow $M = 0.3$. The Helmholtz number of the sound field is $kr_o = 13$. Non-reflecting boundary conditions are imposed on the inlet/outlet section obtained by projecting the solution on the duct modal basis, as described by Casalino *et al.* (2004). The amplitude and phase L2 errors, defined as $\mathrm{Err}_{\mathrm{A}} = \sqrt{\sum_{i=1}^{\mathcal{N}} \left(|p^i| - |p_a^i|\right)^2 / \sum_{i=1}^{\mathcal{N}} |p_a^i|^2}$

N_w	N_r	N_θ	N_z	$\mathrm{Err}_{\mathrm{A}}^{\mathrm{Lilley}}$	$\mathrm{Err}_{\mathrm{P}}^{\mathrm{Lilley}}$	$\mathrm{Err}_{\mathrm{A}}^{\mathrm{Helmholtz}}$	$\mathrm{Err}_{\mathrm{P}}^{\mathrm{Helmholtz}}$
0.29515E+01	5	51	10	0.19894E-02	0.92256E-03	0.19750E-02	0.90009E-03
0.44706E+01	7	75	15	0.79859E-03	0.35116E-03	0.84098E-03	0.34551E-03
0.63108E+01	10	101	20	0.37578E-03	0.15946E-03	0.46310E-03	0.18413E-03
0.78503E+01	12	125	25	0.17319E-03	0.12776E-03	0.17122E-03	0.12635E-03

TABLE 1. Consistency analysis of the GFD method performed by computing the noise transmission through a constant area duct with flow. The L2 error corresponding to the solution of Eq. (2.3), referred to as Lilley, and a convected Helmholtz equation are reported as a function of the average number of nodes per acoustic wavelength N_w. N_r, N_θ, and N_z denote the grid points in the radial, circumferential, and axial directions, respectively.

and $\mathrm{Err}_{\mathrm{P}}=\sqrt{\sum_{i=1}^{\mathcal{N}} \min\{\varphi_1,\varphi_2\}/4\pi^2\mathcal{N}}$, with $\mathcal{N}$ denoting the number of grid points and $\varphi_1 = \left(\arg\left(p^i\right) - \arg\left(p_a^i\right)\right)^2$ and $\varphi_2 = \left(2\pi - \left|\arg\left(p^i\right) - \arg\left(p_a^i\right)\right|\right)^2$, are computed with four axially extruded grids of decreasing size and reported in table 1 as a function of the average number of nodes per acoustic wavelength N_w. Plotting the errors as a function of $1/N_w$ shows that the method is only accurate at second order, since a 27-node stencil is used, but few points per wave are necessary to ensure an acceptable accuracy. Furthermore, in spite of what was expected with the same computational sencil, the higher-order derivatives in Lilley's equation do not affect the global discretization error.

4.2. *Sound scattering by compressible vortices*

The purpose of this test is to verify the discretized Eq. (2.3) in the case of a two-dimensional multidirectional sheared base flow. The model problem of noise scattering by a compressible vortex is solved by computing the linearized Lilley's equation. Results are compared to those obtained by Colonius *et al.* (1994) by using a high-order scheme to solve the Navier-Stokes equations. The present numerical results are obtained by computing the base flow derivatives both numerically, via a least-square approach and a polynomial reconstruction on the acoustic computation grid, and analytically. Two vortex models are considered, the second being more compact and thus characterized by a less sensitive noise refraction to domain truncation errors. Results are presented by plotting the root mean square pressure level of the scattered wave at constant distance from the vortex center. All the results presented have been obtained by using a PML buffer thickness equal to 2λ and a parabolic damping factor with maximum value $\tilde{\sigma}^{\max} = 0.25$. The solution sensitivity to $\tilde{\sigma}^{\max}$ varying in the range $[0.1, 0.75]$ has been checked for the first vortex model, but no significant differences have been observed.

The first vortex model has the following tangential velocity profile:

$$U_\theta = \Gamma\left[1 - \exp\left(-a\, r^2/L^2\right)\right] / (2\pi r) \tag{4.1}$$

where $a \simeq 1.256431$ is such that the maximum velocity occurs at $r = L$, with L denoting the viscous core size. This velocity field mimics an exact solution of the incompressible linear momentum equation (Oseen vortex), provided that $a = L^2/(4\nu t)$, where ν is the kinematic viscosity. Equation (4.1) is also solution for an inviscid compressible flow. For both cases the radial equilibrium requires that $\partial p_0/\partial r = \rho_0 U_\theta^2/r$. Hence, assuming homentropicity ($p_0/\rho_0^\gamma = \text{constant}$), the pressure profile is given by:

$$p_0 = \rho_\infty c_\infty^2\, \gamma^{-1}\left[1 - (\gamma-1)\,\Gamma^2 f\left(a\, r^2/L^2\right) / \left(4c_\infty^2\pi^2 r^2\right)\right]^{\frac{\gamma}{\gamma-1}} \tag{4.2}$$

where $f(x) = 1/2 - \exp(-x) + \exp(-2x)/2 + xE_i(-2x) - xE_i(-x)$, with E_i denoting

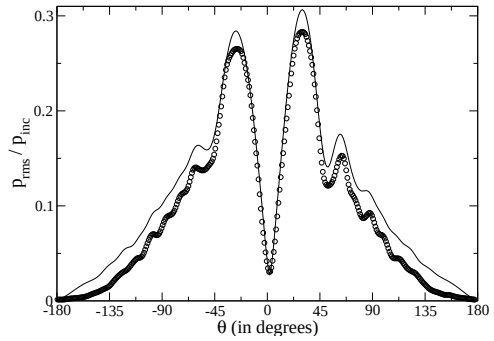

(a) $M_{\max} = 0.0625$. —— : $50L$, ∘ : $40L$.

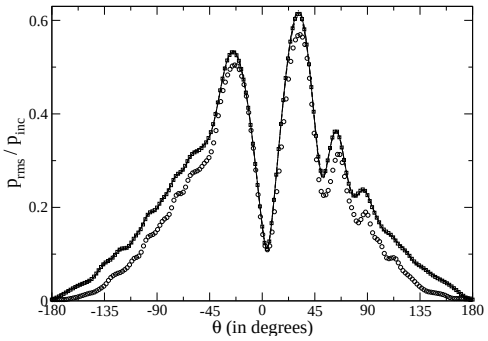

(b) $M_{\max} = 0.125$. —— : $50L$, ∘ : $40L$.

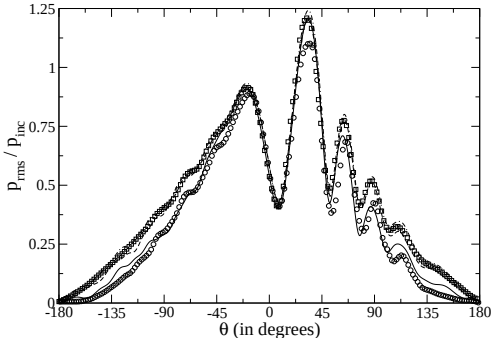

(c) $M_{\max} = 0.25$. —— : $40L$, - - - - : $50L$, – - – : $60L$, ∘ : $40L$, □ : $50L$.

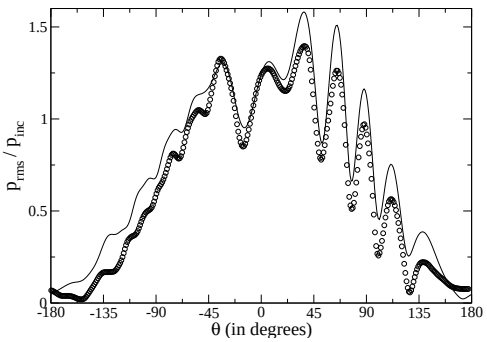

(d) $M_{\max} = 0.5$. —— : $50L$, ∘ : $40L$.

FIGURE 2. Root mean square pressure level of Oseen-vortex scattered wave at $r = 2.5\lambda$ normalized by the incident wave pressure p_{inc}. Comparison between Colonius *et al.* (1994) Navier-Stokes results (symbols) and present Lilley results (lines). In graph (b), Lilley results obtained by using 3 meshes ($L_x = 50L$, $N_x = 321/361/401$) are plotted together with results obtained by computing numerically the base flow derivatives. In graph (c), Lilley results computed on 3 domains ($L_x = 40L/50L/60L$, $N_x = 257/321/385$) with equal mesh spacing are compared to Navier-Stokes computed on 2 domains ($L_x = 40L/50L$).

the exponential integral function. As argued by Colonius *et al.* (1994), this vortex model is a good approximation of an exact viscous compressible solution at the Mach and Reynolds numbers considered. Introducing the dimensionless circulation $\epsilon = \Gamma/(\lambda c_\infty)$ and assuming that $\lambda = 4L$, the maximum induced Mach number is given by $M_{\max} \simeq 0.45539437\,\epsilon$. Computations are performed using four values of $M_{\max}$, for example 0.0625, 0.125, 0.25 and 0.5. A plane wave propagating in the positive x direction is imposed via the radiation condition (2.4) and a PML wave splitting technique. As shown in Fig. 2, discrepancies with respect to the Navier-Stokes results occur, especially when a different domain extension is used. As argued by Colonius *et al.* (1994), this is due to the truncated mean flow refraction effects. In fact, as illustrated in Fig. 2(c), when equivalent domain extensions are used, the present Lilley results and the Navier-Stokes results are in fairly good agreement. Furthermore, Fig. 2(c) shows that increasing the domain size from

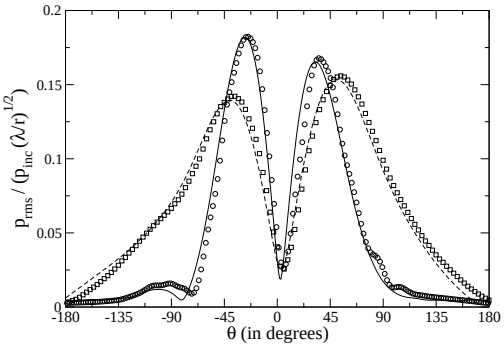

FIGURE 3. Root mean square pressure level of Taylor-vortex scattered wave normalized by $p_{\rm inc}\,(\lambda/r)^{1/2}$. Comparison between Colonius *et al.* (1994) Navier-Stokes results (symbols) and present Lilley results (lines) at different radial distances. —— : $r/\lambda = 2.5$, - - - - : $r/\lambda = 0.5$, $\circ$: $r/\lambda = 2.5$, $\square$: $r/\lambda = 0.5$.

$L_x = 50L$ to $L_x = 60L$ does not affect the present GFD solution significantly. As a final remark, the grid dependence of the GFD solution and its sensitivity to the accuracy of the base flow derivatives have been addressed for the case $M_{\max} = 0.125$. This is shown in Fig. 2(c), where all the GFD curves collapse to one.

The second vortex model is a compact zero circulation swirling flow (Taylor vortex) defined as:

$$U_\theta = U_{\theta\max}\,(r/L)\exp\left[\left(1 - r^2/L^2\right)/2\right], \quad U_r = 0$$

$$p_0 = \rho_\infty c_\infty^2 \gamma^{-1}\left[1-(\gamma-1)\;M_{\max}^2\exp\left(1 - r^2/L^2\right)/2\right]^{\frac{\gamma}{\gamma-1}}, \quad \rho_0 = \rho_\infty\left(\gamma p_0 \rho_\infty^{-1} c_\infty^{-2}\right)^{\frac{1}{\gamma}} \quad (4.3)$$

Again, the scattering of a plane wave is computed for the values $M_{\max} = 0.125$ and $\lambda = 4L$. Of interest in this second computation is that, since this vortex is more concentrated than the first one, the far field domain truncation should not affect the solution remarkably. This is confirmed, as shown in Fig. 3, by the good agreement between present Lilley results (domain size $50L$) and previous Navier-Stokes results (domain size $40L$). The reader should note that, suspecting a post-processing error in the work by Colonius *et al.* (1994), the Navier-Stokes noise directivity for this second case has been plotted by reversing the azimuthal direction. Additionally, the contour levels of the scattered acoustic field are shown in Fig. 4.

4.3. *Sound radiation from a source in a jet flow*

The purpose of this verification test is to stress the capability of the GFD approach in featuring the sound radiation and refraction in the complex aeroacoustic configuration of a source embedded in a high Mach number isobaric Gaussian jet, excited at a frequency in the shear layer instability regime. This test case has been used by Agarwal *et al.* (2004) to demonstrate that the occurrence of vortical instability waves can be avoided by using a direct solver to invert the linear system obtained from the discretization of Lilley's equation in the frequency domain.

Consider a parallel isobaric mean shear flow with Gaussian velocity profile and corresponding Crocco-Busemann density profile:

$$U = U_j \exp\Big(-\ln(2)\,(y/b)^2\Big) \quad (4.4)$$

$$\rho_0 = \rho_j\left[T_\infty/T_j - (T_\infty/T_j - 1)\,U/U_j + (\gamma-1)\,M_j^2\,(U/U_j)\,(1 - U/U_j)/2\right]^{-1} \quad (4.5)$$

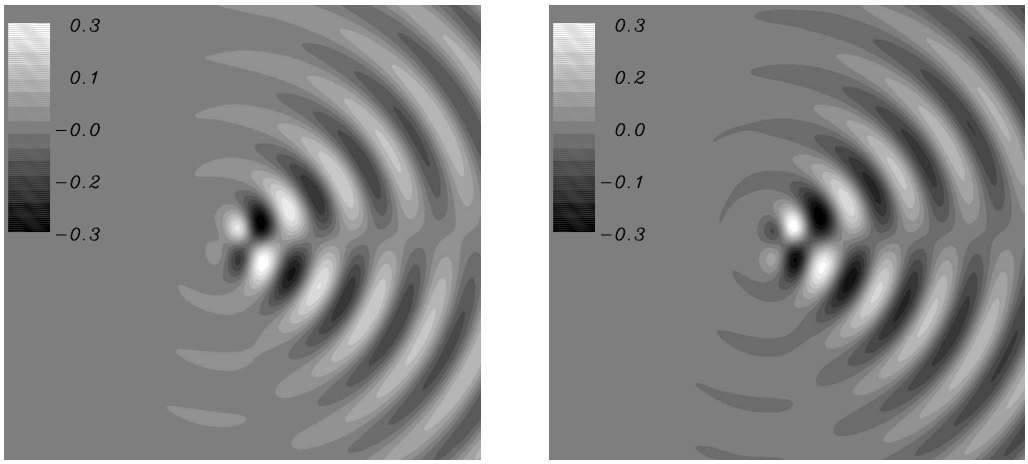

(a) $\mathrm{Re}(p - p_{\mathrm{inc}})$. (b) $\mathrm{Im}(p - p_{\mathrm{inc}})$.

FIGURE 4. Plane wave scattering from a Taylor vortex. Only the physical domain is represented extending over $34L$ in each direction.

where the subscript j denotes jet axis quantities. The mean flow parameters are: $p_0 = p_\infty = 103330\,\mathrm{Pa}$, $M_j = 0.756$, $T_j = 600\,\mathrm{K}$, $T_\infty = 300\,\mathrm{K}$, $\gamma = 1.4$, $R = 287\,\mathrm{m^2\,s^{-2}\,K^{-1}}$, $b = 1.3\,\mathrm{m}$. A dipole-type source $\Lambda(x, y)$ for the linearized energy equation is equivalent to the non-homogeneous linearized Lilley's equation $\mathcal{L}(\Pi') = (\gamma p_0 c_\infty)^{-1} (-\mathrm{i}\, k + \tilde{U}\, \partial/\partial x)^2 \Lambda(x, y)$, where $\mathcal{L}$ denotes the wave operator in Eq. (2.3) and $\Lambda(x, y) = A \exp\left(-B_x x^2 - B_y y^2\right)$, with $A = 0.001\ \mathrm{kg\,m^{-1}\,s^{-3}}$, $B_x = 0.04 \ln(2)\ \mathrm{m^{-2}}$ and $B_y = 0.32 \ln(2)\ \mathrm{m^{-2}}$. The source radian frequency is $\omega = 76\,\mathrm{rad\,s^{-1}}$. Only the half-space $y \geq 0$ is simulated, and a symmetry condition is applied on the line $y = 0$.

As expected for this test case, instability waves were observed when an iterative method was used to solve the governing linear system. Instead of finding the way to control this instabilities, a direct linear system solver has been used, as suggested by Agarwal *et al.* (2004). However, because of serious core memory limitations, computations have been carried out with only three grids, for example 200×200, 200×400, and 400×200. The grid dependence has been checked by considering a computational domain $-100\,\mathrm{m} \leq x \leq 200\,\mathrm{m}$ and $0 \leq y \leq 125\,\mathrm{m}$. A uniform spacing is used along x, and the exponential law $y^j = 125\left[\exp\left(\alpha\eta^j\right) - \exp\left(-\alpha\eta^j\right)\right] / \left[\exp(\alpha) - \exp(-\alpha)\right]$, with η^j varying uniformly from 0 to 1, is used along y. The stretching factor α is taken as 4 and 3 for the coarser and finer grids, respectively. In both cases, this provides about 10 points in the mean shear jet. No significant differences have been observed, thus results are reported only for the coarser grid. The influence of both the domain size and the PML damping factor have been also checked by performing computations for a variety of combinations. Results reported in this section are not dependent from the far field boundary conditions and have been obtained by using a PML buffer thickness equal to 50 m, and a damping factor that increases parabolically from 0 to the maximum value 1.5 at the radiation boundaries, where the modified Sommerfeld condition (2.4) is imposed.

The numerical results are compared to available analytical results obtained by Agarwal *et al.* (2004) along three lines, for example $-50\,\mathrm{m} \leq x \leq 150\,\mathrm{m}$ and $y = 15$, $-50\,\mathrm{m} \leq x \leq 150\,\mathrm{m}$ and $y = 50$, $x = 100$ and $-5\,\mathrm{m} \leq y \leq 50\,\mathrm{m}$. The acoustic pressure at the start

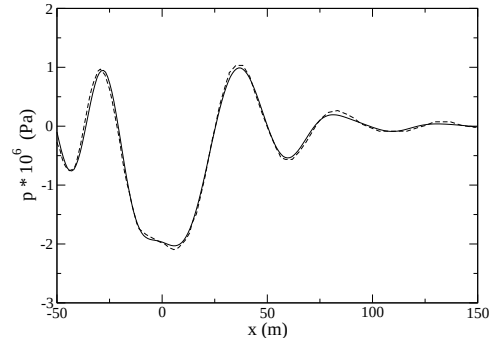

(a) Line $-50\,\mathrm{m} \leq x \leq 150\,\mathrm{m}$ and $y = 15$.

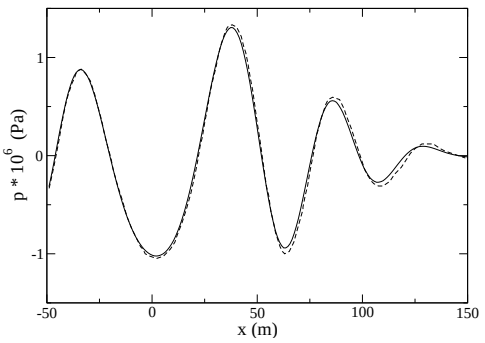

(b) Line $-50\,\mathrm{m} \leq x \leq 150\,\mathrm{m}$ and $y = 50$.

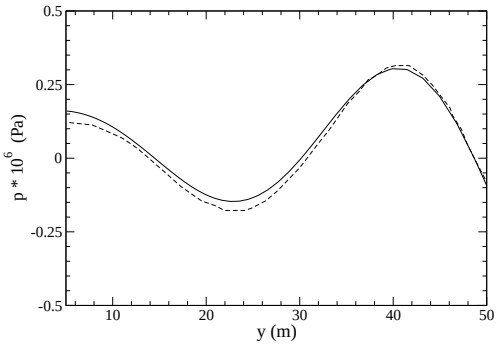

(c) Line $x = 100$, $-5\,\mathrm{m} \leq y \leq 50\,\mathrm{m}$.

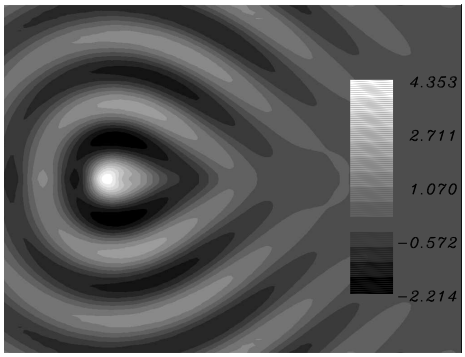

(d) Contour levels in the physical domain.

FIGURE 5. Real part of the acoustic pressure. Comparison between Agarwal *et al.* (2004) analytical results (broken lines) and present Lilley results (lines).

of a cycle (real part) along these three lines is plotted in Fig. 5. The agreement with the analytical solution is fairly good along the three lines.

5. Conclusions

A physical model based on Pridmore-Brown third-order convected wave operator has been implemented in the CAA code GFD. The existing discretization method developed for a second-order wave equation has been extended to the higher order wave equation. A preliminary verification has been carried out in order to check the correctness of both the discretization scheme and the discretized wave equation in the case of a generic multi-directional mean shear flow. Three verification test cases have been considered: the sound transmission through a constant area duct, the scattering of a plane wave from a two-dimensional vortex, and the sound refraction through a two-dimensional shear jet. All the test cases have proved satisfying results. The next step toward a full assessment of the industrial relevance of the GFD method for sound radiation from a realistic turbofan exhaust consists of computing the sound diffraction at a trailing edge in the presence of flow.

REFERENCES

Agarwal, A., Morris, P. J. & Mani, R. 2004 Calculation of sound propagation in nonuniform flows: suppression of instability waves. *AIAA Journal* **42** (1), 80–88.

Bécache, E., Dhia, A. S. B.-B. & Legendre, G. 2004 Perfectly matched layers for the convected helmholtz equation. *SIAM Journal on Numerical Analysis* **42** (1), 409–433.

Berenger, J. P. 1994 A perfectly matched layer for the absorption of electromagnetic waves. *Journal of Computational Physics* **114**, 185–200.

Bergliaffa, S. E. P., Hibberd, K., Stone, M. & Visser, M. 2004 Wave equation for sound in fluids with vorticity. *Physica D* **191**, 121–136.

Caruthers, J. E., French, J. C. & Raviprakash, G. K. 1995*a* Green's function discretization for numerical solution of the helmholtz equation. *Journal of Sound and Vibration* **187** (4), 553–568.

Caruthers, J. E., French, J. C. & Raviprakash, G. K. 1995*b* Recent developments concerning a new discretization method for the helmholtz equation. *AIAA Paper 95-117*.

Casalino, D., Genito, M. & Visingardi, A. 2006 Numerical analysis of noise scattering effects due to the airframe in tilt rotor systems. *AIAA Paper 2006-2608*.

Casalino, D., Roger, M. & Jacob, M. 2004 Prediction of sound propagation in ducted potential flows using green's function discretization. *AIAA Journal* **42** (4), 736–744.

Colonius, T., Lele, S. K. & Moin, P. 1994 The scattering of sound waves by a vortex - numerical simulations and analytical solutions. *Journal of Fluid Mechanics* **260**, 271–298.

Colonius, T., Lele, S. K. & Moin, P. 1997 Sound generation in a mixing layer. *Journal of Fluid Mechanics* **330**, 375–409.

Di Francescantonio, P. & Casalino, D. 1999 Green's function discretization scheme for sound propagation in nonuniform flows. *AIAA Journal* **37** (10), 1161–1172.

Druon, Y., Lidoine, S. & Roger, M. 2004 Acoustic radiation modeling of engine exhaust. Comparison between analytical and numerical methods. *AIAA Paper 2004-2990*.

Freund, J. B., Lele, S. K. & Wei, M. 2004 The robustness of acoustic analogies. Proceedings of the 2004 Summer Program, Center for Turbulence Research, NASA Ames/Stanford Univ., 241–252.

Hu, F. Q. 2004 Absorbing boundary condition. *SIAM Journal on Numerical Analysis* **18** (6), 513–522.

Hu, F. Q. 2005 A perfectly matched layer absorbing boundary condition for linearized Euler equations with a non-uniform mean flow. *Journal of Computational Physics* **208**, 469–492.

Lilley, G. M. 1974 On the noise from jets. *AGARD CP-131*.

Pierce, A. D. 1990 Wave equation for sound in fluids with unsteady inhomogeneous flow. *Journal of the Acoustical Society of America* **87** (6), 2292–2299.

Pridmore-Brown, D. C. 1958 Sound propagation in a fluid flowing through an attenuating duct. *Journal of Fluid Mechanics* **4**, 393–406.